Over-the-air Computation for Cooperative Wideband Spectrum Sensing and Performance Analysis

Li Chen, Nan Zhao, *Senior Member, IEEE,* Yunfei Chen, *Senior Member, IEEE,*
F. Richard Yu, *Fellow, IEEE,* and Guo Wei

***Abstract*—For sensor network aided cognitive radio, cooperative wideband spectrum sensing can distribute the sampling and computing pressure of spectrum sensing to multiple *sensor nodes* (SNs). However, this may incur high latency due to distributed data fusion, especially when the number of SNs is large. In this paper, we propose a novel cooperative wideband spectrum sensing scheme using over-the-air computation. Its key idea is to utilize the superposition property of wireless channel to implement the summation of Fourier transform. This avoids distributed data fusion by computing the target function directly. The performance of the proposed scheme is analyzed with imperfect synchronization between different SNs considered. Furthermore, a *synchronization phase offset* (SPO) estimation and equalization method is proposed. The corresponding performance after equalization is also derived. Both a working prototype based on *universal software radio periphera* (USRP) and Monte Carlo simulations are provided to verify the performance of the proposed scheme.**

***Index Terms*—cooperative sensing, cognitive radio, imperfect synchronization, over-the-air computation, wireless sensor network**

I. Introduction

Due to the spectrum shortage caused by the ever-increasing demand for higher data rate, cognitive radio has become a prominent solution by allowing unlicensed use of vacant licensed spectrum with dynamic access. A critical functionality to enable spectrum sharing is spectrum sensing. Different spectrum sensing methods have been proposed in the literature. For example, spectrum sensing has been fully investigated based on energy detection [1], [2] and other second-order statistic features [3], [4].

Compared with narrowband spectrum sensing, wideband spectrum sensing is more challenging due to the Nyquist sampling theory. Also, the Fourier transform over a large amount of sampled data requires a strong computing ability of the *sensor nodes* (SNs) [5]. When the sampling and computing ability is limited, the wideband spectrum can be divided into multiple narrow ones, and the SN senses one at a time with the help of reconfigurable bandpass filter and tunable oscillator [6], [7]. Such scheme sacrifices the real-time ability for high speed sampling and large data computing. When the band locations and their widths are known in advance, Landau has demonstrated a minimal rate requirement that equals to the sum of the bandwidths, which is below the corresponding Nyquist rate [8]. A wideband spectrum sensing scheme based on multicoset sampling was also proposed in [9], which is a nonuniform sub-Nyquist sampling technique and can be realized using an efficient multi-channel architecture. H. Hassanieh *et al.* proposed the use of sparse Fourier transforms to reconstruct a sparse spectrum in realtime without sampling it at the Nyquist rate [10]. Y. Chen *et al.* conducted a survey of the state-of-the-art spectrum occupancy models in [11].

Among these works, compressive sensing has been widely studied as a popular sub-Nyquist sensing technology, since the wideband spectrum is typically underutilized, or sparse in the frequency domain. Compressive sensing was first introduced in wideband spectrum sensing in [12], where the number of the compressed measurements was determined by the sparsity level of the spectrum. Without prior knowledge of the sparsity level, a two-step compressed sensing scheme was proposed in [13]. It estimated the actual sparsity level first and then adjusted the number of compressed measurements. H. Sun *et al.* proposed an iterative method to adaptively adjust the number of compressed measurements for wideband spectrum sensing in [14]. The output of geolocation database was utilized to reduce the computation complexity and improve the detection performance [15], [16]. X. Zhang *et al.* proposed an efficient adaptively-regularized iterative algorithm to implement wideband spectrum compressive sensing [17]. Although compressive sensing can recovery the spectrum at sub-Nyquist rate, it requires random sampling of the signal through analog mixing at Nyquist rates [18], which cannot be achieved using standard low-speed *analog to digital converters* ADCs. Also, to recover the original signal from the compressed measurements requires an optimization problem, which usually incurs high computation complexity. Therefore, it is difficult to implement compressed sensing at SNs with limited sampling and computing abilities.

When multiple SNs are available, cooperative spectrum sensing can provide both spatial diversity gain and multi-node sampling gain. The sensing performance of a single SN may degrade due to fading and shadowing. By exploiting spatial diversity from multiple SNs, a cooperative spectrum sensing based on hard combining was investigated in [19], where SNs performed compressive sensing individually but shared binary decisions with each other. Different from the hard combining

L. Chen and G. Wei are with Department of Electronic Engineering and Information Science, University of Science and Technology of China. (e-mail: {chenli87, wei}@ustc.edu.cn).

N. Zhao is with the School of Info. and Commun. Eng., Dalian University of Technology, Dalian, China (email: zhaonan@dlut.edu.cn).

Y. Chen is with the School of Engineering, University of Warwick, Coventry CV4 7AL, U.K. (e-mail: Yunfei.Chen@warwick.ac.uk).

F.R. Yu is with the Department of Systems and Computer Engineering, Carleton University, Ottawa, ON, K1S 5B6, Canada (email: richard.yu@carleton.ca).

with one-bit decision, a soft-combining cooperative network was proposed in [20], where the original autocorrelation of the compressed signal was collected from each SN by the *fusion center* (FC). H. Guo *et al.* provided a linear combination rule to minimize the probability of missed detection subject to an upper limit on the probability of false alarm [21]. Furthermore, multiple SNs can be also utilized to reduce the sampling requirement of wideband spectrum sensing known as parallel spectrum sensing, where each node senses a particular band and the wideband spectrum estimation can be collected from multiple SNs [22], [23]. The time allocation for sensing duration and communication duration was optimized in [24] for parallel spectrum sensing. Y. Wang *et al.* first discussed a tradeoff between the spatial diversity achieved by cooperation and the sampling gain achieved by parallel sensing in [25]. To jointly collect both diversity gain and sampling gain, they developed a novel cooperative spectrum sensing technique based on matrix rank minimization.

Although the sampling complexity can be reduced through parallel sampling, it requires multiple access scheme to avoid the inter-node interference during distributed data fusion, e.g. *time division multiple access* (TDMA) or *carrier sense multiple access* (CSMA), which incurs a high latency especially when the number of SNs is large. Classical methods to reduce the latency are limiting the number of cooperative nodes through opportunistic scheduling [26], [27] or jointing source channel coding to compress the data volume [28], [29]. Interference alignment as a promising technique for interference management has been applied to spectrum sharing in cognitive radios [30], [31]. However, the scheduling overhead and orthogonal resources allocation are high.

Motivated by the above observations, we propose a cooperative wideband spectrum sensing scheme using over-the-air computation for sensor network aided cognitive radio. It utilizes the superposition property of wireless channel to implement the summation of Fourier transform in order to avoid distributed data fusion and compute the target function directly. The spectrum signal is sampled by multiple SNs in an interleaving way, which reduces the requirements on both sampling and computing. After calculating the modified *discrete fourier transformation* (DFT) at each SN individually, the estimated spectrum of the FC is combined through the wireless channel and hence referred to as over-the-air computation. Since the scheme focuses on the combined spectrum rather than individual SNs', the proposed scheme harnesses the interference rather than avoiding it. The superposition property of wireless channel is widely used in coherent distributed estimation [32], compute-and-forward relay [33], and structured function computing [34]. Various experimental platforms have been built to verify the idea of over-the-air computation in [35], [36]. To the best of our knowledge, applying over-the-air computation to Fourier transform has never been discussed before. We also built a prototype based on *universal software radio peripheral* (USRP) software radios to verify the proposed scheme. The contributions can be summarized as follows.

- (**Spectrum sensing using over-the-air computation**) A cooperative wideband spectrum sensing scheme using over-the-air computation is proposed, which utilizes the superposition property of wireless channel to implement the summation of Fourier transform. It avoids distributed data fusion and computes the target function directly.
- (**The impact of SPO and noise**) By considering *synchronization phase offset* (SPO) between different SNs, the corresponding estimated spectrum with aliasing effect is provided. Based on the defined *signal to aliasing and noise ratio* (SANR), the SANR for both uniform distributed SPO and Gaussian distributed SPO is derived.
- (**The SPO estimation and equalization**) In order to compensate the impact of imperfect synchronization, an SPO estimation and equalization method is designed. The performance of the SANR after equalization is derived with the residual error considered.

Compared with compressive sensing, our method does not need the spectrum sparse and the sparsity level known. Also, it does not require random sampling ADC and optimization problem computation at the SN. And compared with parallel sensing, our method avoids distributed data fusion and fully utilizes the superposition property of wireless channel to implement over-the-air computation for Fourier transform.

The remainder of this paper is organized as follows. Section II presents the system model about wideband spectrum sensing. The designed scheme is proposed in Section III. The impact of imperfect synchronization and its corresponding equalization design are provided in Section IV. Experimental and numerical results are given in Section V. Conclusion is provided in VI.

II. System Model

In this work, we consider a cooperative sensor network aided cognitive radio as illustrated in Fig.1. A dedicated sensor network with L spatially distributed SNs indexed by $l \in \{0, 1, \cdots, L-1\}$ monitors the spectrum and reports the observations to the *cognitive user* (CU). From the sensor-aided network point of view, CU can be also regarded as the FC of the network. The CU/FC recovers the spectrum and performs the occupancy decision. There are two assumptions of the model.

- **Assumption 1**: Considering a dense sensor network, whose size is much smaller than the distance between the network and the *primary user* (PU), the spectrum observed by SNs and the CU/FC is assumed to be the same.
- **Assumption 2**: For sensor network aided cognitive radio, the CU/FC is only interested in some specific sub-bands of the wideband, but the sensor node SN should have the ability to sense a wideband in order to serve various CUs.

The spectrum source $x(t)$ is assumed to be band-limited, and its *continuous Fourier transform* (CFT) is

$$S_{\mathcal{F}}(\Omega) = \mathcal{F}[x(t)] = \int_{-\infty}^{\infty} x(t)\, e^{-j\Omega t} dt, \tag{1}$$

where $S_{\mathcal{F}}(\Omega) = 0$ when $\Omega < -\Omega_0$ or $\Omega > \Omega_0$. Applying uniform sampling to $x(t)$ with period T_0, $x(t)$ can be sampled

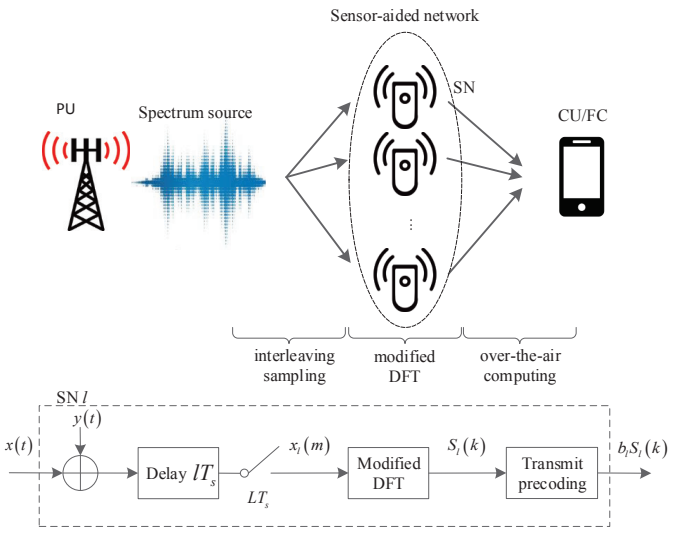

Figure 1. The system model

as a discrete sequence $x[n] = x(nT_0)$ and the observe noise during sampling stage is expresses as $y(t)$.

In order to avoid spectrum aliasing, the sampling rate should obey the Nyquist rate, i.e., $1/T_0 \geq \Omega_0/\pi$. Assuming the sequence length of $x[n]$ is N, the corresponding DFT of $x[n]$ can be calculated as

$$S(k) = \sum_{n=0}^{N-1} x[n] e^{-j\frac{2\pi nk}{N}}, k \in [0, 1, \cdots, N-1]. \quad (2)$$

For wideband spectrum with large Ω_0, it is hard to satisfy the Nyquist sampling rate. Meanwhile, the corresponding computation complexity with large N is also high. The direct implementation of DFT using (2) requires $\mathcal{O}(N^2)$ operations. Using *fast fourier transform* (FFT) to compute (2) needs $\mathcal{O}(N \log N)$ operations [37].

III. Sensing Using Over-the-air Computation

For wideband spectrum sensing, the SNs are constrained to their limited sampling and computing abilities. In order to distribute the sampling and computing load to multiple SNs, we propose a cooperative wideband spectrum estimation scheme through distributed sensing and over-the-air computing, which can be realized by a set of low-cost and low-power SNs.

A. Distributed sensing

From the time domain's point of view, one way to relax the requirement of sampling is letting multiple SNs sample $x(t)$ in an interleaved way. Specifically, the sampling sequence of SN l is

$$x_l[m] = x(mLT_0 + lT_0) + y_l[m], \quad (3)$$

where $m \in \{0, 1, \cdots, M-1\}$, $M = N/L$ and $y_l[m]$ is the observation noise at SN l after sampling [1]. The sampling sequences at all SNs can be put together as the original sequence of spectrum source. In this way, the requirement for the sampling process at each SN is relaxed by a factor of L.

From the frequency domain's point of view, $S(k)$ in (2) considering observe noise can be written as

$$\begin{aligned} S_1(k) &= \sum_{m=0}^{M-1} \sum_{l=0}^{L-1} x_l[m] e^{-j\frac{2\pi k}{N}(mL+l)} \\ &= \sum_{l=0}^{L-1} [S_l(k) + Y_l(k)] \\ &= S(k) + Y(k), \end{aligned} \quad (4)$$

where $S_l(k)$ is the modified DFT of $x_l[m]$ as

$$S_l(k) = \sum_{m=0}^{M-1} x_l[m] e^{-j\left(\frac{2\pi k}{M}m + \frac{2\pi kl}{N}\right)}, \quad (5)$$

and

$$S(k) = \sum_{l=0}^{L-1} S_l(k). \quad (6)$$

Similarly, $Y_l(k)$ is the modified DFT of $y_l[m]$, and $Y(k) = \sum_{l=0}^{L-1} Y_l(k)$.

This method relaxes the sampling requirement and decreases the computational complexity at each SN.

Proposition 1. (**The computational complexity of modified DFT**) The direct implementation of the modified DFT in (5) requires $\mathcal{O}(MN)$ operations. Utilizing FFT to compute (5), the operations are reduced to $\max\{\mathcal{O}(M \log M), \mathcal{O}(N)\}$.

Proof. If we implement the modified DFT directly to calculate (5), we would need one M-dimensional inner product for each $k \in \{0, 1, \cdots, N-1\}$. Each inner product consists of M multiplications and $M-1$ additions. Hence, one inner product takes $\mathcal{O}(M)$ operations. We have to do N of them, meaning that the total number of operations needed through the direct way to calculate (5) is $\mathcal{O}(MN)$.

In order to utilize FFT to compute the modified DFT, (5) can be rewritten as

$$S_l(k) = e^{-j\frac{2\pi kl}{N}} \sum_{m=0}^{M-1} x_l[m] e^{-j\frac{2\pi km}{M}}, \quad (7)$$

which is composed of the FFT of $x_l[m]$ and a multiplication. For all $k \in \{0, 1, \cdots, N-1\}$, the total number of operations needed for multiplication is $\mathcal{O}(N)$. Meanwhile, the total number of operations needed for the FFT of $x_l[m]$ is $\mathcal{O}(M \log M)$. Thus, the total number of operations through FFT to calculate (5) is $\max\{\mathcal{O}(M \log M), \mathcal{O}(N)\}$. □

It is worth noting that the implementation of the interleaved sampling faces several practical issues. One is the synchronization of all SNs through clock sharing. The most straightforward sharing clock is to connect a single external clock to SNs clock input via wires. While, this way eliminates the *synchronization frequency offset* (SFO), it also prevents

[1] In our work, we assume that sensing time of SN is generally several orders of magnitude longer than the channel coherence time. Thus, only path loss and shadowing are considered for channel models. Different SNs experience similar path-loss effects and spatially correlated shadowing effects.

mobility and flexibility. An alternative solution, called AirShare, was developed in [38] for synchronizing sensors by broadcasting a reference-clock signal and its effectiveness demonstrated using a prototype. While, this way can eliminate the roots of SFO, but *synchronization phase offset* (SPO) is inevitable. In the Section IV, we will discuss the impact of SPO, and provide an SPO estimation and equalization method.

B. Over-the-air computing

After distributed sensing, each SN has its own $S_l(k)$. In order to recover the spectrum, we can adopt the traditional "aggregate-then-compute" way, which aggregates $S_l(k)$ from all SNs then computes the estimated spectrum according to (4). However, this requires multiple access for the SNs (e.g. TDMA, CSMA) in order to avoid interference during distributed data fusion, which incurs a high latency especially when the number of SNs is large.

In the proposed scheme, we utilize the summation property of wireless channel to compute (4) over-the-air. Assuming all SNs transmit their own sensing results with perfect synchronization, the received spectrum at the FC can be expressed as

$$S_2(k) = \sum_{l=0}^{L-1} h_l b_l \left[S_l(k) + Y_l(k)\right] + Z(k), \tag{8}$$

where $h_l \in \mathcal{C}$ is the wireless channel between SN l and the FC, $b_l \in \mathcal{C}$ is the precoding scalar of SN l, and $Z(k)$ is the received noise.

In order to compensate the non-uniform fading between different SNs, a uniform-forcing precoding scalar b_l can be designed based on each SN's own *channel state information* (CSI)[2], i.e.,

$$b_l = \frac{\sqrt{\eta} {h_l}^*}{|h_l|^2}, \tag{9}$$

where η is the uniform power level. Considering a transmit power constraint at each SN, i.e., $|b_l|^2 \le P_{\max}$, η can be calculated as

$$\eta = P_{\max} \min_l \left\{|h_l|^2\right\}, \tag{10}$$

which depends on the minimum channel power gain of all SNs. We design a novel signaling procedure utilizing the "OR" property of the wireless channel to determine η which avoids aggregating all SNs CSI. The signaling procedure is illustrated in Fig. 2, which is composed of 3 steps.

- **Step 1 (Local CSI estimation and quantization)**: Each SNs estimates the CSI h_l between itself and the FC based on the pilot broadcasted by the FC. Then each SN calculates and quantizes $1/|h_l|^2$ into a binary representation as

$$\frac{1}{h_l} = \sum_{b=-b_L}^{b_M} \nu_b 2^b, \tag{11}$$

where $\nu_b \in \{0, 1\}$, b_M is the *most significant bit* (MSB) and b_L is the *least significant bit* (LSB). MSB is determined by the possible maximum value of $1/|h_l|^2$ and LSB is determined by the tolerable quantized error.

- **Step 2 (Determine significant bit one by one)**: The FC uses several rounds of inquiry from MSB b_M to LSB b_L in order to determine the $\max_l\{1/|h_l|^2\}$, i.e., $\min_l\{|h_l|^2\}$. In the first inquiring round, SNs with 1 in the MSB respond, while SNs with 0 in the MSB keep silent. The FC detects the signal to determine whether the MSB of $\max_l\{1/|h_l|^2\}$ is 1. If so, the MSB of $\max_l\{1/|h_l|^2\}$ is set as 1. Otherwise, it is set as 0. In the second inquiring round, if MSB is set as 1, the FC inquires the SNs with MSB as 1 whether they have 1 in the second MSB. Otherwise, the FC inquires all IoT devices whether they have 1 in the second MSB. Then the second MSB is determined.
- **Step 3 (η calculation and broadcasting)**: The FC inquires in this way until the LSB is determined. Then $\max_l\{1/|h_l|^2\}$, i.e., $\min_l\{|h_l|^2\}$, can be determined. After calculating $\eta = P_{\max}\min_l\{|h_l|^2\}$, the FC broadcasts the η to all SNs.

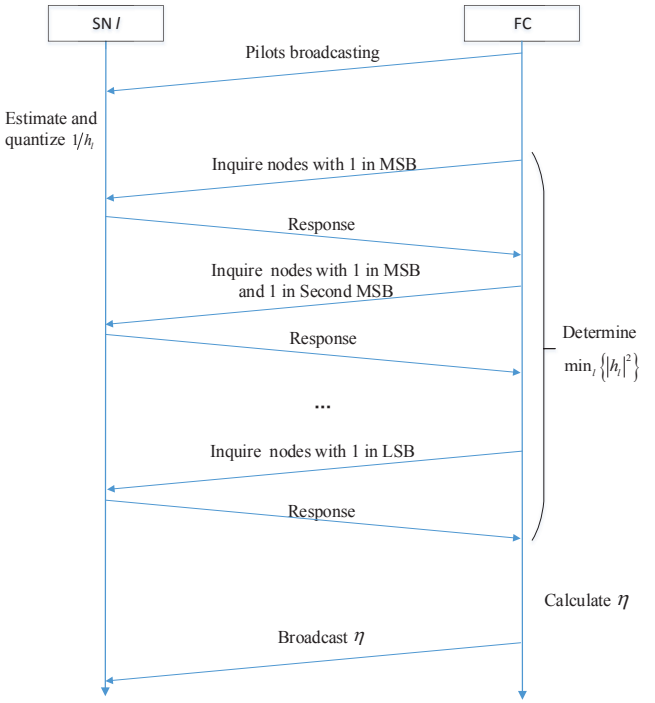

Figure 2. The signaling procedure to determine η

Then the received spectrum considering both observed noise and received noise can be rewritten as

$$\begin{aligned} S_2(k) &= \sqrt{\eta}\sum_{l=0}^{L-1}\left[S_l(k) + Y_l(k)\right] + Z(k) \\ &= \sqrt{\eta}S(k) + \sqrt{\eta}Y(k) + Z(k). \end{aligned} \tag{12}$$

In conclusion, the proposed scheme of wideband spectrum estimation through distributed sensing and over-the-air com-

[2]We can use channel reciprocity to allow each SN to measure its channel to the FC with very low overhead. Note that the forward and reverse channels are always the same since they operate on the same carrier frequency in *time division duplex* (TDD) systems.

Algorithm 1 Spectrum sensing through distributed sensing and over-the-air computing

- **Step 1** (**Sampling in an interleaved way**): L SNs sample $x(t)$ in an interleaving way, where SN l samples $x(t)$ with the sampling period LT_0 and the sampling delay lT_0 to get the sampling sequence $x_l[m]$ in (3).
- **Step 2** (**Modified DFT in a distributed way**): The modified DFT $S_l(k)$ in (5) is computed at SN l with the sampling sequence $x_l[m]$ from Step 1. SNs perform modified DFT to compute $S_l(k)$ in a distributed way.
- **Step 3** (**Computation over-the-air**): After precoded by b_l in (9), all SNs transmit $S_l(k)$ with perfect synchronization. The estimated spectrum $S_2(k)$ in (12) is received at the FC, which is combined over-the-air.

puting is summarized in Algorithm 1. The advantages of the proposed scheme can be summarized as follows.

- (**Low sampling requirement**) The sampling requirement of each SN decreases from $1/T_0$ to $1/LT_0$. The more SNs cooperate to sense spectrum, the lower sampling rate is required, which can be realized by a set of cheap and low-power SNs.
- (**Low computation complexity**) The computation complexity of each SN decreases from $\mathcal{O}(N^2)$ to $\mathcal{O}(MN)$ with DFT and from $\mathcal{O}(N\log N)$ to $\max\{\mathcal{O}(M\log M), \mathcal{O}(N)\}$ with FFT, respectively, which decreases the computing requirement of SNs.
- (**Low sensing latency**) The proposed scheme avoids distributed data fusion which incurs a high latency of the reporting channels. It takes advantage of the wireless channel superposition property to realize the summation of Fourier transform over-the-air efficiently.

IV. Imperfect Synchronization

The proposed scheme can distribute the sampling and computing load to multiple SNs and compute the estimated spectrum over-the-air efficiently. However, the SNs may not be perfectly synchronized. In this section, we analyze the impact of the SPO. Furthermore, we propose an estimation and equalization method to compensate the impact.

A. The impact of imperfect synchronization

Two related issues are usually considered for an imperfect synchronization. One is SPO, which is caused by the misaligned initial clock instants between different SNs. The other is SFO, which is caused as different SNs are driven by independent clocks. In this paper, we only consider the SPO between different SNs, because SFO can be avoided when SNs share a common reference clock.

A random SPO of SN l is assumed to be Φ_l, which is caused by misaligned initial instants of the reference clock for both sampling and transmitting. Then the received spectrum with SPO at the FC in (12) can be rewritten as

$$S_3(k) = \sqrt{\eta}\sum_{l=0}^{L-1} e^{j\Phi_l} S_l(k) + Y_l(k) + Z(k). \tag{13}$$

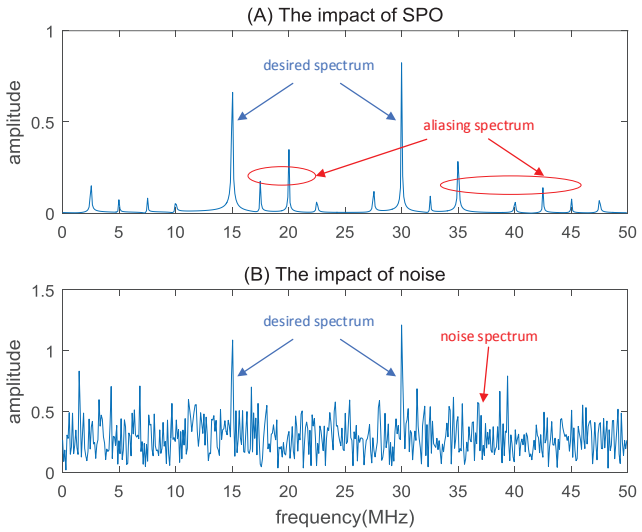

Figure 3. The received spectrum with SPO and noise. The source spectrum is $x(t) = \sin(f_1 x) + 2\sin(f_2 x)$, $f_1 = 15$ MHz, and $f_2 = 30$ MHz. The number of SN $L = 8$ and the sampling frequency for each SN is 12.5 MHz.

The impact of SPO to the received spectrum can be given by Proposition 2.

Proposition 2. (The received spectrum with SPO) The received spectrum $S_3(k)$ with SPO in (13) can be rewritten as

$$\begin{aligned} S_3(k) = &\underbrace{\sqrt{\eta}\alpha(0) S_{\mathcal{F}}\left(\frac{2\pi k}{NT_0}\right)}_{\text{desired spectrum}} + \sqrt{\eta}Y(k) + Z(k) \\ &+ \underbrace{\sqrt{\eta}\sum_{i=1}^{L-1}\alpha(i) S_{\mathcal{F}}\left(\frac{2\pi k}{NT_0} - \frac{2\pi i}{LT_0}\right)}_{\text{aliasing spectrum}} \end{aligned} \tag{14}$$

where

$$\alpha(i) = \frac{1}{L}\sum_{l=0}^{L-1} e^{j\Phi_l} e^{-jl\frac{2\pi i}{L}}, i \in \{0, 1, \cdots, L-1\}, \tag{15}$$

$S_{\mathcal{F}}(\Omega)$ is given in (1).

Proof. The Proposition 2 is proved in Appendix A. □

Remark 1. (**The impact of SPO and noise**) According to Proposition 2, the received spectrum at the FC is composed of the desired spectrum, the aliasing spectrum caused by SPO, the observe noise and the receive noise. An example of the received spectrum with SPO and noise is shown in Fig.3, where a sinusoidal spectrum signal is assumed.

Remark 2. (**The combined power of** $\alpha(i)$) Actually $\alpha(i)$ in (15) can be regarded as L-DFT of $e^{j\Phi_l}/L$. Then according to Parsevals theorem, the combined power of $\alpha(i)$ can be calculated as

$$\sum_{i=0}^{L-1}|\alpha(i)|^2 = L\sum_{l=0}^{L-1}\left|e^{j\Phi_l}/L\right|^2 = 1. \tag{16}$$

Remark 3. (**The $\alpha(i)$ without SPO**) If all SNs are perfectly synchronized without SPO, i.e., $\Phi_l = 0, l \in [0, \cdots, L-1]$. According to (15), we have that

$$\alpha(i) = \begin{cases} 1 & i = 0 \\ 0 & i \in \{1, \cdots, L-1\} \end{cases}. \tag{17}$$

Then the received spectrum $S_3(k)$ in (13) with SPO is equal to $S_2(k)$ in (12) without SPO.

In order to provide quantitative analysis of the impact of SPO and noise, we define the SANR as follows. Furthermore, the probability of detection and the probability of false alarm can be derived based on the defined SANR [39].

Definition 1. (**SANR**) The SANR can be defined as

$$\gamma_S = \frac{P_D}{P_A + N_O + N_R}, \tag{18}$$

where P_D is the power of the desired spectrum, P_A is the power of the aliasing spectrum, N_O is the observe noise power and N_R is the receive noise power.

According to Definition 1, the SANR of the received spectrum in (14) can be calculated as

$$\gamma_S = \frac{\mathrm{E}\left(|\alpha(0)|^2\right) P}{\mathrm{E}\left(\sum_{i=1}^{L-1} |\alpha(i)|^2\right) P + N_O + N_R/\eta} \tag{19}$$

where P is the spectrum signal power, $\mathrm{E}(|\alpha(0)|^2)P$ is the desired spectrum power, $\mathrm{E}(\sum_{i=1}^{L-1}|\alpha(i)|^2)P$ is the aliasing spectrum power, and η is the uniform power control level in (10). The expression of SANR is given in the following proposition.

Proposition 3. (**The SANR with SPO and noise**) For the proposed spectrum estimation scheme, the SANR considering SPO and noise in (19) can be calculated as

$$\gamma_S = \frac{1 + (L-1)\varphi_{\Delta_\Phi}(1)}{L - [1 + (L-1)\varphi_{\Delta_\Phi}(1)] + L\gamma_O{}^{-1} + L(\eta\gamma_R)^{-1}}, \tag{20}$$

where $\gamma_O = S/N_O$ is the *signal to observe noise power ratio* (SONR), $\gamma_R = S/N_R$ is the *signal to receive noise power ratio* (SRNR), $\Delta_\Phi = \Phi_l - \Phi_m$ is the difference of SPO between different SNs, and $\varphi_{\Delta_\Phi}(t) = \mathrm{E}\left(e^{jt\Delta_\Phi}\right)$ is the characteristic function of Δ_Φ.

Proof. The Proposition 3 is proved in Appendix B. □

Remark 4. (**The upper bound of the SANR**) Because the characteristic function $\varphi_{\Delta_\Phi}(t)$ is bounded as $|\varphi_{\Delta_\Phi}(t)| \le 1$, the upper bound of the SANR is

$$\gamma_S^{(\text{upper})} = \frac{1}{\gamma_O{}^{-1} + (\eta\gamma_R)^{-1}}. \tag{21}$$

Actually, the upper bound of γ_S is the SANR without SPO.

Remark 5. (**The SANR with uniform SPO**) Assuming that the difference of SPO between SNs satisfies uniform distribution, i.e., $\Delta_\Phi \sim \mathcal{U}(-a, a)$, we have that

$$\varphi_{\Delta_\Phi}(t) = \frac{\sin ta}{ta} = \mathrm{sinc}(ta). \tag{22}$$

Then $\varphi_{\Delta_\Phi}(1) = \mathrm{sinc}(a)$. And the corresponding SANR is

$$\gamma_S^{(\text{uniform})} = \frac{[1 + (L-1)\,\mathrm{sinc}(a)]}{L - [1 + (L-1)\,\mathrm{sinc}(a)] + L\gamma_O{}^{-1} + L(\eta\gamma_R)^{-1}}. \tag{23}$$

Remark 6. (**The SANR with Gaussian SPO**) Assuming that the difference of SPO between SNs satisfies Gaussian distribution, i.e., $\Delta_\Phi \sim \mathcal{N}\left(0, \sigma_\Phi^2\right)$, we have that

$$\varphi_{\Delta_\Phi}(t) = e^{-t\sigma_\Phi^2/2}. \tag{24}$$

Then $\varphi_{\Delta_\Phi}(1) = e^{-\sigma_\Phi^2/2}$. And the corresponding SANR is

$$\gamma_S^{(\text{Gaussian})} = \frac{\left[1 + (L-1)\,e^{-\frac{\sigma_\Phi^2}{2}}\right]}{L - \left[1 + (L-1)\,e^{-\frac{\sigma_\Phi^2}{2}}\right] + L\gamma_O{}^{-1} + L(\eta\gamma_R)^{-1}}. \tag{25}$$

If energy detection is adopted to decide whether the sub-band is occupied or not, the performance of the detector in terms of its *receiver operating characteristics* (ROC) curve can be given as follows.

Proposition 4. (**The ROC with energy detection**) Given the received spectrum at the FC in (14), the probability of detection $\mathcal{P}_D$ can be expressed as a function of the probability of false alarm $\mathcal{P}_F$, i.e.,

$$\mathcal{P}_D = 1 - F_{\chi_2^2}\left(\frac{F_{\chi_2^2}{}^{-1}(1 - \mathcal{P}_F)}{1 + \gamma_S}\right) \tag{26}$$

where $F_{\chi_2^2}(\cdot)$ is the cumulative distribution function (CDF) of chi-squared distributed variable with 2 degrees of freedom χ_2^2.

Proof. The Proposition 4 is proved in Appendix C. □

B. SPO Estimation and Equalization

In order to compensate the impact of SPO, we design an SPO estimation and equalization method to improve the performance of the proposed scheme. As illustrated in Fig.4, the method is composed of 3 stages.

- **Step 1 (Broadcasting sinusoidal pilot signal)** The FC broadcasts a strong and known sinusoidal pilot signal $Ae^{j\Omega_0 t}$ whose Fourier transform is $2\pi A\delta(\Omega - \Omega_0)$ to all SNs. Because each SN has the CSI h_l between itself and the FC, the received sinusoid signal at each SN is equivalent to $Ae^{j\Omega_0 t}$ after post-processing by $1/h_l$. Also, compared with the spectrum signal, the broadcasting pilot is strong. Thus, we can neglect the spectrum signal, the observe noise and the receive noise.
- **Step 2 (Recovering the spectrum of pilot signal)** The pilot signal is recovered through distributed sensing and over-the-air computing scheme proposed in Algorithm 1. The estimated spectrum of the pilot signal at the FC can

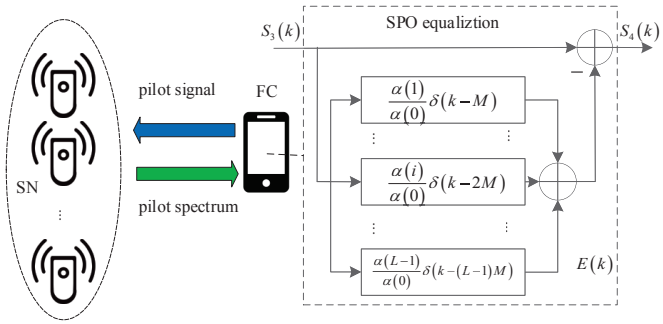

Figure 4. The SPO estimation and equalization

Algorithm 2 The SPO estimation and equalization method

- **Step 1 (Pilot broadcasting)**: The FC broadcasts a strong and known sinusoidal pilot signal $Ae^{j\Omega_0 t}$ to all SNs. The received sinusoid signal at each SN is equivalent to $Ae^{j\Omega_0 t}$ after post-processing by $1/h_l$.
- **Step 2 (SPO estimation)**: The estimated spectrum through distributed sensing and over-the-air computing is (27), where $\alpha(i)$ and their corresponding SPO Φ_l can be estimated.
- **Step 3 (Aliasing equalization)**: The aliasing error can be reconstructed through an $L-1$ taps FIR filter in (28), and the equalized results are the estimated spectrum subtracting the reconstructed aliasing spectrum.

be given according to (14) with spectrum noise neglected, i.e.,

$$S_{\text{pilot}}(k) = 2\pi A\sqrt{\eta}\sum_{i=0}^{L-1}\alpha(i)\delta\left(\frac{2\pi k}{NT_0}-\frac{2\pi i}{LT_0}\right), \quad (27)$$

where $\alpha(i)$ is given in (15), which composed of the desired spectrum line at $i=0$, and aliasing spectrum line at $i=1,2,\cdots,L-1$ with the amplitude $\alpha(i)$. As is illustrated in Remark 2, $\alpha(i)$ can be regarded as DFT of $e^{j\Phi_l}/L$. With measured $\alpha(i)$, we can get Φ_l through IDFT of $\alpha(i)$.

- **Step 3 (The SPO equalization at the FC)** In order to avoid the Φ_l feedback, an equalizer is designed to eliminate the aliasing spectrum at the FC. The basic idea of equalization is to reconstruct the aliasing error and subtract it from the output signal. Then the desired signal can be obtained. The aliasing error can be reconstructed through an $L-1$ taps FIR filter as illustrated in Fig.4, i.e.,

$$E(k) = \sum_{i=1}^{L-1}\frac{\alpha(i)}{\alpha(0)}\delta(k-Mi), \quad (28)$$

Then the equalized results are the estimated spectrum subtracting the reconstructed aliasing spectrum.

In conclusion, the proposed SPO estimation and equalization method is summarized in Algorithm 2. It is worth noting that an intuitive way to eliminate SPO impact after the SPO estimation is feeding back the SPO to SNs. Then each SN adjusts its phase or does a pre-equalization which can fully eliminate the SPO theoretically. However, the feedback incurs redundant communication cost, especially when the number of SNs is large.

In order to avoid the feedback, we design the equalizer at the FC based on the estimated SPO. The aliasing spectrum can be perfect reconstructed at the FC if we have the desired spectrum $S(k)$. Unfortunately, we do not have $S(k)$ at the FC but the received spectrum $S_3(k)$ in (13) with aliasing error and noise. The only way is using $S_3(k)$ instead, which will incur residual error due to the original error.

C. Performance after equalization

With the equalizer designed in (28), the output spectrum after equalization can be given as

$$\begin{aligned} S_4(k) =& S_3(k) - S_3(k) * E(k) \\ =& \sqrt{\eta}\alpha(0) S_{\mathcal{F}}\left(\frac{2\pi k}{NT_0}\right) \\ &\underbrace{-\sqrt{\eta}\sum_{i=1}^{L-1}\alpha(i) S_{\mathcal{F}}\left(\frac{2\pi k}{NT_0}-\frac{2\pi i}{LT_0}\right) * E(k)}_{\text{residual error caused by aliasing spectrum}} \\ &\underbrace{-[\sqrt{\eta}Y(k)+Z(k)] * [E(k)-1]}_{\text{residual error caused by noise}} \end{aligned} \quad (29)$$

where $S_3(k)$ and $E(k)$ are given in (14) and (28) respectively.

Remark 7. (**The upper bound of SANR after equalization**) The ideal equalization will eliminate all aliasing spectrum causing by SPO and the corresponding upper bound of SANR is

$$\gamma_S^{(\text{eq,up})} \le \frac{\mathrm{E}\left(|\alpha(0)|^2\right)P}{N_O + N_R/\eta}. \quad (30)$$

Proposition 5. (**The lower bound of SANR after equalization**) The lower bound of SANR after equalization can be given as

$$\gamma_S^{(\text{e,l})} \ge \frac{\mathrm{E}\left(|\alpha(0)|^2\right)P}{\Lambda^2(L)\,\mathrm{E}\left(\sum_{i=1}^{L-1}|\alpha(i)|^2\right)P + [\Lambda^2(L)+1]\left(N_O+\frac{N_R}{\eta}\right)}, \quad (31)$$

where

$$\Lambda(L) = \mathrm{E}\left(\sum_{i=1}^{L-1}\left|\frac{\alpha(i)}{\alpha(0)}\right|\right). \quad (32)$$

Proof. The Proposition 5 is proved in Appendix D. □

Remark 8. (**The equalization gain**) Compared with the SANR before equalization in (19), when the observe noise power N_O and receive noise N_R are relatively small, the equalization gain can be approximated as

$$G \ge \frac{\gamma_S^{(\text{e,l})}}{\gamma_S} \approx \frac{1}{\Lambda^2(L)} \quad (33)$$

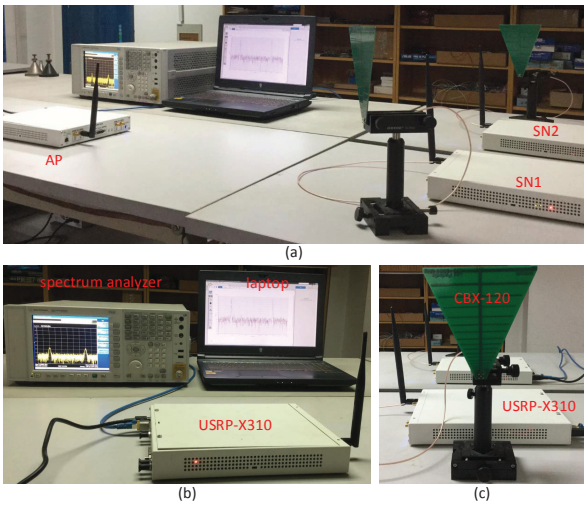

Figure 5. The experimental platform

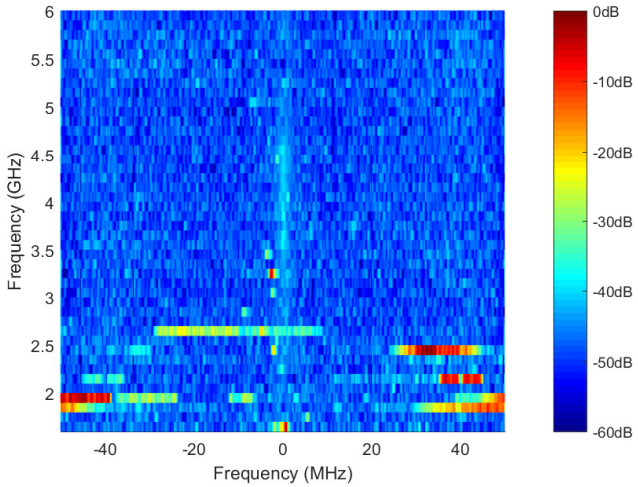

Figure 6. The estimated spectrum form 1 GHz to 6 GHz.

The equalization gain $G \geq 1$, when $\Lambda^2(L) \leq 1$. It means that we can get an improvement in SANR after equalization if $\alpha(i)$ caused by the SPO, the observe noise and receive noise are all relatively small. That also means the better the initial performance, the better the equalization performance.

Remark 9. (**The cascading equalization**) When $G \geq 1$, a better SANR can be further achieved by cascading the equalizer, which means the equalization can be realized by multiple stages, and the equalized output in this stage is used as the equalized input in the next stage. Similar to Proposition 4, the lower bound of SANR after K stages equalization can be given as

$$\gamma_S^{(\mathrm{e,l})} \geq \frac{\mathrm{E}\left(|\alpha(0)|^2\right) P}{\Lambda^{2K}(L)\,\mathrm{E}\left(\sum_{i=1}^{L-1}|\alpha(i)|^2\right) P + [\Lambda^{2K}(L)+1]\left(N_O + \frac{N_R}{\eta}\right)} \tag{34}$$

And the corresponding equalization gain with relatively small observe noise power and receive noise power is

$$G \geq \frac{\gamma_S^{(\mathrm{e,l})}}{\gamma_S} \approx \frac{1}{\Lambda^{2K}(L)} \tag{35}$$

V. Numerical Results and Discussion

A. Experimental results

We built an experimental platform using universal software radio peripheral (USRP) platform to verify the proposed spectrum sensing scheme. The USRP platform is well-known for its low-cost and high-quality realization of software-defined-radio, which provides various functionalities to efficiently realize wireless system that operates in the RF band.

The experimental platform is composed of 2 SNs and 1 FC as illustrated in Fig.5(a). The FC is shown in Fig.5(b), which is composed of a 2.4 GHz narrowband antenna to receive the estimated spectrum from SNs, a USPR X310 to convert the received signal to the digital one, a PC to show the estimated spectrum and a spectrum analyzer to reveal the exact spectrum.

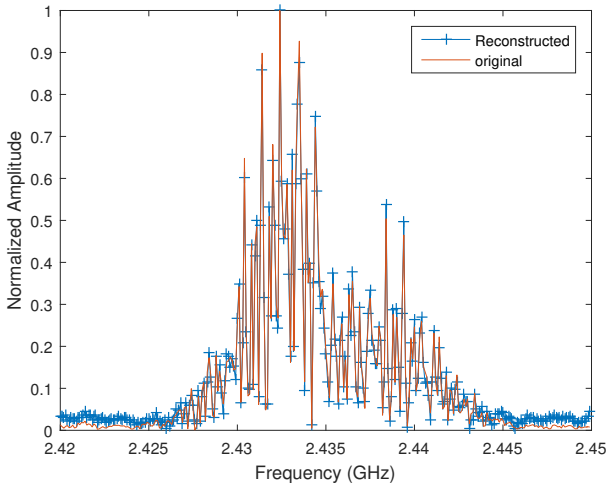

Figure 7. The estimated spectrum from 2.42 GHz to 2.45 GHz

The USRP is connected to the PC through ethernet port. The output spectrum is shown through NI LabView on the PC. The SN is shown in Fig.5(c), which is composed of a wideband antenna (CBX-120: 1.2 GHz∼6 GHz) for spectrum sensing, a USPR X310 to sample the signal then do modified DFT, and a 2.4 GHz narrowband antenna to transmit the distributed sensing results. The transmit symbol rate is 1 M symbol/sec with I/Q channels.

The reconstructed spectrum form 1 GHz to 6 GHz is shown in Fig.6 [3], where the details from 2.42 GHz to 2.45 GHz is also shown and compared to the spectrum sensing results of the spectrum analyzer in Fig.7. The accuracy of the reconstructed spectrum is evaluated by the relative reconstruction mean squared error (r-MSE). Compared with the spectrum measured by the spectrum analyzer. The r-MSE is defined as

[3]Each block represents a 1 MHz bandwidth frequency band and the color of the block represents the normalized power of the frequency band. The frequency of the each band can be calculated based on the summation of x-axe value and y-axe value.

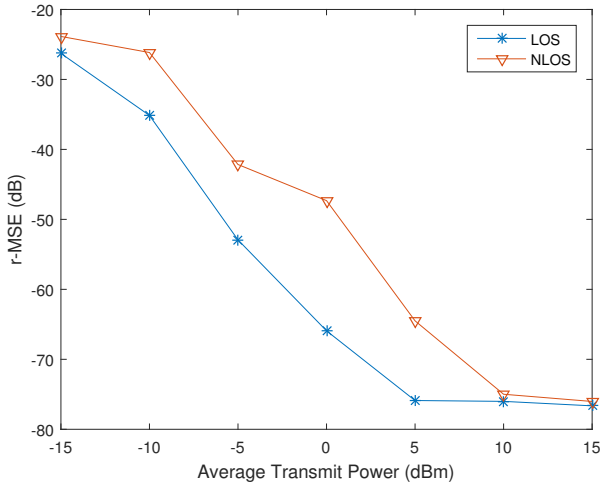

Figure 8. The r-MSE between estimated spectrum and that of spectrum analyzer

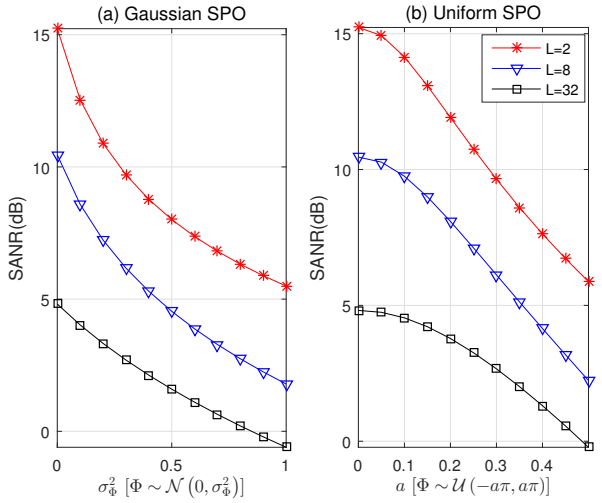

Figure 9. The SANR with SPO

$$\text{r-MSE} = \frac{\|S'(k) - S(k)\|}{\|S(k)\|}, \tag{36}$$

where the reference of the measurement is made by the spectrum analyzer as shown in Fig.5(b). The r-MSE of the reconstructed spectrum (2.42 GHz∼2.45 GHz) versus different average transmit power (-15 dBm∼15 dBm) is given in Fig.8. The distances between FC and SNs are fixed to 5m. Both line-of-sight (LOS) scenario and non-line-of-sight (NLOS) scenario are evaluated. It can be seen that the r-MSE decreases when the transmit power increases, and that the performance of LOS has 5 dB gain over that of NLOS.

B. Monte-Carlo simulation

In order to illustrate the expected performance of the proposed scheme, we adopt Monte-Carlo simulations of 10^5 times. The SONR and SRNR are given as $\gamma_O = 20$ dB and $\gamma_R = 20$ dB, respectively. Different numbers of SNs $L = 2, 8, 32$ are simulated.

In Fig.9, the SANR considering SPO is shown, where both Gaussian distributed SPO and uniformly distributed SPO are simulated. In Fig.9(a), the Gaussian SPO of different SNs $\Phi \sim \mathcal{N}(0, \sigma_\Phi^2)$ and its variance $\sigma_\Phi^2 = 0 \sim 0.5$. It can be seen that the increase of σ_Φ^2 will decrease the SANR, and the decreasing rate decreases with the increase of σ_Φ^2. In Fig.9(b), the uniform SPO of different SNs $\Phi \sim \mathcal{U}(-a\pi, a\pi)$ and its scale $a = 0 \sim 0.5$. It can be seen that the increase of a will decrease the SANR, and the decreasing rate is almost the same. When the number of SNs increases, the SANR decreases. That is because the impact of SPO will be intensified with more SNs.

The SANR after equalization with different cascading numbers ($K = 1, 3$) is shown in Fig.10. It is compared with the SANR without equalization and the equalization benchmark, i.e., the upper-bound SANR without residual error. Both uniformly distributed SPO and Gaussian distributed SPO are given. The number of SNs is $L = 8$. It can be seen that the equalization can improve the average SANR especially

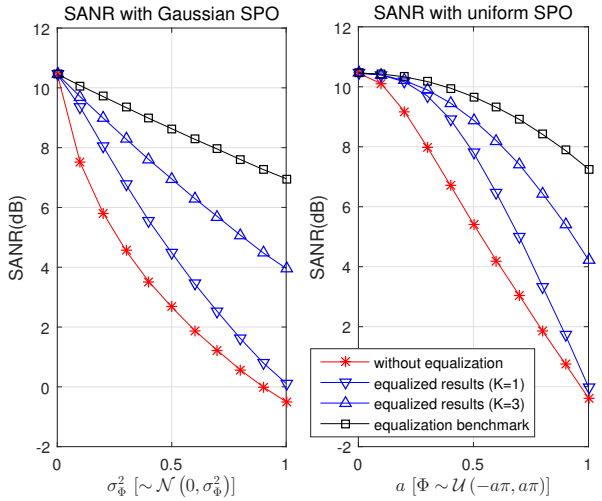

Figure 10. The average SANR with equalization

when the SPO is small. While, as the SPO increases, the performance gain between the equalized results and the results without equalization decreases, and the performance gap between the equalization benchmark and the equalized results increases. That is because the residual error after equalization increases with the increase of SPO. While, the performance gain between equalization with $K = 1$ and equalization with $K = 3$ increases as the SPO increases. It means that the cascading equalization is beneficial to reduce the residual error.

The ROC curve with energy detection is shown in Fig.11, where the detection probability $\mathcal{P}_D$ is the function of the false alarm probability $\mathcal{P}_F$. The SPO is Gaussian distributed as $\Phi \sim \mathcal{N}(0, 1)$. The number of SN is $L = 8$. The performance of equalization with different cascading numbers ($K = 1, 3$) is compared with the performance without equalization and the performance benchmark, i.e., the perfect equalization without residual error. Both the simulated results and the theoretical performances are compared. The simulated performances without equalization is almost the same with the theoretical

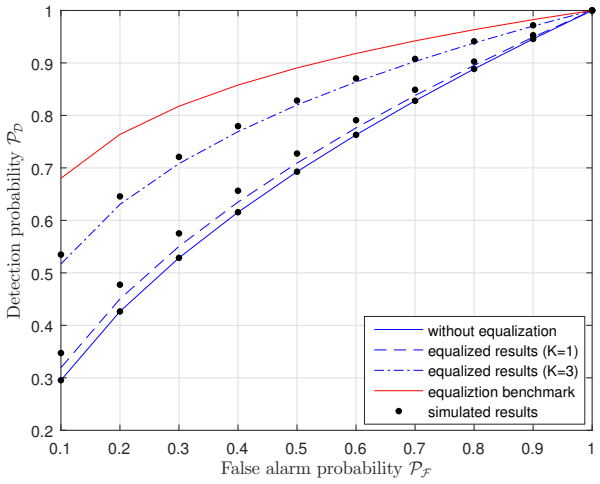

Figure 11. The ROC curve withe energy detection

performances without equalization, which verifies the accuracy of the theoretical analysis. While, the simulated performances of equalization is better than the theoretical performances. That is because we derive the theoretical results based on the lower bound of SANR after K stages equalization. It can be seen that the equalization can improve the ROC performance, especially with cascading equalization.

VI. Conclusion

In this work, we have proposed a novel cooperative spectrum sensing via over-the-air computation for sensor network aided cognitive radio, which does not only distribute the sampling and computing pressure to multiple SN but also avoids a high latency during distributed data fusion. Multiple SNs are employed to sample the wideband spectrum signal in an interleaving way. The modified DFT is computed at each SNs locally. The estimated spectrum is combined at the FC through over-the-air computing, which fully utilizes the superposition property of the wireless channel. The impact of imperfect synchronization between SNs is analyzed. And a corresponding SPO estimation and equalization method is also proposed. The improved performance after equalization is further derived. An experimental prototype has been built to verify the proposed scheme based on USRP. Monte Carlo simulation is also provided to illustrate its expected performance.

Appendix A
Proof of Proposition 2

The sampling sequence of SN l can be rewritten as

$$\begin{aligned} x_l[m] &= x(mT_0 + lT_0) \\ &= x(t - lT_0) \cdot \sum_{m=-\infty}^{\infty} \delta(t - mT_0). \end{aligned} \tag{37}$$

Then the Fourier transforms of $x_l[m]$ can be calculated as

$$\begin{aligned} S_{\mathcal{F},l}(\Omega) &= \mathcal{F}\{x_l[m]\} \\ &= \frac{1}{2\pi} \cdot \mathcal{F}\{x(t - lT_0)\} * \mathcal{F}\left\{\sum_{m=-\infty}^{\infty} \delta(t - mT_0)\right\}, \end{aligned} \tag{38}$$

where

$$\mathcal{F}\{x(t - lT_0)\} = e^{-jl\Omega T_0} S_\mathcal{F}(\Omega) \tag{39}$$

and

$$\mathcal{F}\left\{\sum_{m=-\infty}^{\infty} \delta(t - mT_0)\right\} = \frac{2\pi}{LT_0} \sum_{i=-\infty}^{\infty} \delta\left(\Omega - \frac{2\pi i}{LT_0}\right). \tag{40}$$

Then

$$S_{\mathcal{F},l}(\Omega) = \frac{1}{LT_0} \sum_{i=-\infty}^{\infty} e^{-jl\frac{2\pi i}{L}} S_\mathcal{F}\left(\Omega - \frac{2\pi i}{LT_0}\right). \tag{41}$$

The summation of $S_{\mathcal{F},l}$ with the phase offset Φ_l can be calculated as

$$\sum_{l=0}^{L-1} e^{j\Phi_l} S_{\mathcal{F},l}(\Omega) = \frac{1}{LT_0} \sum_{l=0}^{L-1} e^{j\Phi_l} \sum_{i=-\infty}^{\infty} e^{-jl\frac{2\pi i}{L}} S_\mathcal{F}\left(\Omega - \frac{2\pi i}{LT_0}\right), \tag{42}$$

which is a periodic function of i with a period L. Considering a period $i \in [0, 1, \cdots, L-1]$, the spectrum of $i = 0$ is the desired spectrum, and the spectrum of $i \in [1, \cdots, L-1]$ is aliasing spectrum. Then it can be rewritten as

$$\sum_{l=0}^{L-1} e^{j\Phi_l} S_{\mathcal{F},l}(\Omega) = \alpha(0) S_\mathcal{F}(\Omega) + \sum_{i=1}^{L-1} \alpha(i) S_\mathcal{F}\left(\Omega - \frac{2\pi i}{LT_0}\right), \tag{43}$$

where

$$\alpha(i) = \frac{\sqrt{\eta}}{L} \sum_{l=0}^{L-1} e^{j\Phi_l} e^{-jl\frac{2\pi i}{L}}, i \in \{0, 1, \cdots, L-1\}. \tag{44}$$

Because the DFT $S(k)$ is the CFT with $\Omega = 2\pi k / NT_0$, the received spectrum in (13) can be calculated as

$$S_3(k) = \sqrt{\eta} \sum_{l=1}^{L} e^{j\Phi_l} S_{\mathcal{F},l}\left(\frac{2\pi k}{NT_0}\right) + \sqrt{\eta} Y(k) + Z(k). \tag{45}$$

According to (43) and (45), it completes the proof.

Appendix B
Proof of Proposition 3

According to the definition of $\alpha(i)$ in (15), $|\alpha(0)|^2$ can be calculated as

$$
\begin{aligned}
|\alpha(0)|^2 &= \frac{1}{L^2}\left|\sum_{l=0}^{L-1} e^{j\Phi_l}\right|^2 \\
&= \frac{1}{L^2}\sum_{l=0}^{L-1} e^{j\Phi_l}\sum_{m=0}^{L-1} e^{-j\Phi_m} \\
&= \frac{1}{L^2}\left[L+\sum_{l=0}^{L-1}\sum_{m\neq l} e^{j(\Phi_l-\Phi_m)}\right] \\
&= \frac{1}{L^2}\left[L+\sum_{l=0}^{L-1}\sum_{m\neq l} e^{j\Delta_\Phi}\right].
\end{aligned} \tag{46}
$$

Then the expectation of $|\alpha(0)|^2$ can be calculated as

$$
\begin{aligned}
\mathrm{E}\left[|\alpha(0)|^2\right] &= \frac{1}{L^2}\left[L+\sum_{l=0}^{L-1}\sum_{m\neq l}\mathrm{E}\left(e^{j\Delta_\Phi}\right)\right] \\
&\overset{(a)}{=} \frac{1}{L}\left[1+(L-1)\,\varphi_{\Delta_\Phi}(1)\right],
\end{aligned} \tag{47}
$$

where the procedure (a) is according to the definition of characteristic function $\varphi_{\Delta_\Phi}(t)=\mathrm{E}\left(e^{jt\Delta_\Phi}\right)$. According to the combined power of $\alpha(i)$ in (16), we have

$$
\mathrm{E}\left[\sum_{i=1}^{L-1}|\alpha(i)|^2\right] = 1-\frac{1}{L}\left[1+(L-1)\,\varphi_{\Delta_\Phi}(1)\right], \tag{48}
$$

which completes the proof.

Appendix C
Proof of Proposition 4

The wideband spectrum is divided into K sub-bands. We test the following binary hypotheses to decide whether the k-th sub-band is occupied or not, i.e.,

$$
\begin{aligned}
&\mathcal{H}_{0,k}: S_3(k) = N_e(k) \\
&\mathcal{H}_{1,k}: S_3(k) = S(k) + N_e(k)
\end{aligned} \tag{49}
$$

where $N_e(k)$ is the effective noised composed of aliasing spectrum, the observe noise and the receive noise. $S(k)$ and $N_e(k)$ are assumed to be Gaussian distributed, i.e., $S(k)\sim\mathcal{CN}(0,P_D)$ and $N_e(k)\sim\mathcal{CN}(0,P_A+P_O+P_R)$ according to Definition 1. The energy detector measures the energy of the received signal of a particular sub-band and compares it to a predetermined threshold, i.e.,

$$
|S_3(k)|^2 \underset{\mathcal{H}_{0,k}}{\overset{\mathcal{H}_{1,k}}{\gtrless}} \Gamma_k, \forall k \tag{50}
$$

where Γ_k is the decision threshold of sub-band k, and $|S_3(k)|^2$ is chi-squared distributed with 2 degrees of freedom, which gives the probability of false alarm as

$$
\begin{aligned}
\mathcal{P}_F &= \Pr\left(|S_3(k)|^2 > \Gamma_k\,|\mathcal{H}_{0,k}\right) \\
&= 1-F_{\chi_2^2}\left(\frac{2\Gamma_k}{P_A+N_O+N_R}\right),
\end{aligned} \tag{51}
$$

and the probability of detection as

$$
\begin{aligned}
\mathcal{P}_D &= \Pr\left(|R_k|^2 > \Gamma_k\,|\mathcal{H}_{1,k}\right) \\
&= 1-F_{\chi_2^2}\left(\frac{2\Gamma_k}{P_D+P_A+N_O+N_R}\right) \\
&= 1-F_{\chi_2^2}\left(\frac{{F_{\chi_2^2}}^{-1}(1-\mathcal{P}_F)}{1+\gamma_{SANR}}\right).
\end{aligned} \tag{52}
$$

It completes the proof.

Appendix D
Proof of Proposition 3

The Fourier transforms of $E(k)$ is

$$
\mathcal{F}[E(k)] = \sum_{i=1}^{L-1}\frac{\alpha(i)}{\alpha(0)}e^{-j\omega 2\pi iM}. \tag{53}
$$

Then we have the following inequality.

$$
|\mathcal{F}[E(k)]| = \left|\sum_{i=1}^{L-1}\frac{\alpha(i)}{\alpha(0)}e^{-j\omega 2\pi iM}\right| \le \sum_{i=1}^{L-1}\left|\frac{\alpha(i)}{\alpha(0)}\right|. \tag{54}
$$

The signal power after equalization can be calculated according to the principle that the convolution in time domain is the product in frequency domain. Considering the output after equalization in (29), the power of the residual aliasing spectrum has an upper bound as

$$
\mathrm{E}^2\left[|\mathcal{F}[E(k)]|\right]P_A \le \mathrm{E}^2\left[\sum_{i=1}^{L-1}\left|\frac{\alpha(i)}{\alpha(0)}\right|\right]\mathrm{E}\left(\sum_{i=1}^{L-1}|\alpha(i)|^2\right)P. \tag{55}
$$

And the power of the residual observe noise and receive noise in (29) also has an upper bound as

$$
\begin{aligned}
&\left[\mathrm{E}^2\left(|\mathcal{F}[E(k)]|\right)+1\right]\left(N_O+\frac{N_R}{\eta}\right) \\
&\le\left[\mathrm{E}^2\left(\sum_{i=1}^{L-1}\left|\frac{\alpha(i)}{\alpha(0)}\right|\right)+1\right]\left(N_O+\frac{N_R}{\eta}\right).
\end{aligned} \tag{56}
$$

Then the lower bound of SANR in (31) can be given.

References

[1] A. Margoosian, J. Abouei, and K. N. Plataniotis, "An accurate kernelized energy detection in gaussian and non-gaussian/impulsive noises," *IEEE Trans. Signal Process.*, vol. 63, no. 21, pp. 5621–5636, Nov 2015.

[2] Y. Ye, Y. Li, G. Lu, and F. Zhou, "Improved energy detection with laplacian noise in cognitive radio," *IEEE Systems J.*, vol. PP, no. 99, pp. 1–12, 2017.

[3] C. Liu, H. Li, and M. Jin, "Blind central-symmetry-based feature detection for spatial spectrum sensing," *IEEE Trans. Veh. Technol.*, vol. 65, no. 12, pp. 10 147–10 152, Dec 2016.

[4] C. Guo, S. Chen, and F. Liu, "Polarization-based spectrum sensing algorithms for cognitive radios: Upper and practical bounds and experimental assessment," *IEEE Trans. Veh. Technol.*, vol. 65, no. 10, pp. 8072–8086, Oct 2016.

[5] A. P. Diguez, M. Amor, J. Lobeiras, and R. Doallo, "Solving large problem sizes of index-digit algorithms on gpu: Fft and tridiagonal system solvers," *IEEE Trans. Comput.*, vol. 67, no. 1, pp. 86–101, Jan 2018.

[6] H. Joshi, H. H. Sigmarsson, S. Moon, D. Peroulis, and W. J. Chappell, "High-q fully reconfigurable tunable bandpass filters," *IEEE Trans. Microw. Theory Techn.*, vol. 57, no. 12, pp. 3525–3533, Dec 2009.

[7] L. Luo, N. M. Neihart, S. Roy, and D. J. Allstot, "A two-stage sensing technique for dynamic spectrum access," *IEEE Trans. Wireless Commun.*, vol. 8, no. 6, pp. 3028–3037, June 2009.

[8] H. J. Landau, "Necessary density conditions for sampling and interpolation of certain entire functions," *Acta Math.*, vol. 117, pp. 37–52, 1967. [Online]. Available: https://doi.org/10.1007/BF02395039

[9] P. Feng and Y. Bresler, "Spectrum-blind minimum-rate sampling and reconstruction of multiband signals," in *1996 IEEE International Conference on Acoustics, Speech, and Signal Processing Conference Proceedings*, vol. 3, May 1996, pp. 1688–1691 vol. 3.

[10] H. Hassanieh, L. Shi, O. Abari, E. Hamed, and D. Katabi, "Ghz-wide sensing and decoding using the sparse fourier transform," in *2014 IEEE Conference on Computer Communications*, April 2014, pp. 2256–2264.

[11] Y. Chen and H. S. Oh, "A survey of measurement-based spectrum occupancy modeling for cognitive radios," *IEEE Commun. Surveys Tuts.*, vol. 18, no. 1, pp. 848–859, Firstquarter 2016.

[12] Z. Tian and G. B. Giannakis, "Compressed sensing for wideband cognitive radios," in *2007 IEEE International Conference on Acoustics, Speech and Signal Processing*, vol. 4, April 2007, pp. IV–1357–IV–1360.

[13] Y. Wang, Z. Tian, and C. Feng, "Sparsity order estimation and its application in compressive spectrum sensing for cognitive radios," *IEEE Trans. Wireless Commun.*, vol. 11, no. 6, pp. 2116–2125, June 2012.

[14] H. Sun, W. Y. Chiu, and A. Nallanathan, "Adaptive compressive spectrum sensing for wideband cognitive radios," *IEEE Commun. Lett.*, vol. 16, no. 11, pp. 1812–1815, November 2012.

[15] Z. Qin, Y. Gao, and C. G. Parini, "Data-assisted low complexity compressive spectrum sensing on real-time signals under sub-nyquist rate," *IEEE Trans. Wireless Commun.*, vol. 15, no. 2, pp. 1174–1185, Feb 2016.

[16] Y. Ma, X. Zhang, and Y. Gao, "Joint sub-nyquist spectrum sensing scheme with geolocation database over tv white space," *IEEE Trans. Veh. Technol.*, vol. PP, no. 99, pp. 1–1, 2017.

[17] X. Zhang, Y. Ma, Y. Gao, and S. Cui, "Real-time adaptively-regularized compressive sensing in cognitive radio networks," *IEEE Trans. Veh. Technol.*, vol. PP, no. 99, pp. 1–1, 2017.

[18] E. J. Candes, J. Romberg, and T. Tao, "Robust uncertainty principles: exact signal reconstruction from highly incomplete frequency information," *IEEE Trans. Inf. Theory*, vol. 52, no. 2, pp. 489–509, Feb 2006.

[19] Z. Tian, "Compressed wideband sensing in cooperative cognitive radio networks," in *2008 IEEE Global Telecommunications Conference*, Nov 2008, pp. 1–5.

[20] Y. Wang, A. Pandharipande, Y. L. Polo, and G. Leus, "Distributed compressive wide-band spectrum sensing," in *2009 Information Theory and Applications Workshop*, Feb 2009, pp. 178–183.

[21] H. Guo, W. Jiang, and W. Luo, "Linear soft combination for cooperative spectrum sensing in cognitive radio networks," *IEEE Commun. Lett.*, vol. 21, no. 7, pp. 1573–1576, July 2017.

[22] Z. Quan, S. Cui, A. H. Sayed, and H. V. Poor, "Optimal multiband joint detection for spectrum sensing in cognitive radio networks," *IEEE Trans. Signal Process.*, vol. 57, no. 3, pp. 1128–1140, March 2009.

[23] P. Paysarvi-Hoseini and N. C. Beaulieu, "Optimal wideband spectrum sensing framework for cognitive radio systems," *IEEE Trans. Signal Process.*, vol. 59, no. 3, pp. 1170–1182, March 2011.

[24] R. Caromi, Y. Xin, and L. Lai, "Fast multiband spectrum scanning for cognitive radio systems," *IEEE Trans. Commun.*, vol. 61, no. 1, pp. 63–75, January 2013.

[25] Y. Wang, Z. Tian, and C. Feng, "Collecting detection diversity and complexity gains in cooperative spectrum sensing," *IEEE Trans. Wireless Commun.*, vol. 11, no. 8, pp. 2876–2883, August 2012.

[26] Z. Zhang, X. Wen, H. Xu, and L. Yuan, "Sensing nodes selective fusion scheme of spectrum sensing in spectrum-heterogeneous cognitive wireless sensor networks," *IEEE Sensors J.*, vol. 18, no. 1, pp. 436–445, Jan 2018.

[27] M. Zheng, L. Chen, W. Liang, H. Yu, and J. Wu, "Energy-efficiency maximization for cooperative spectrum sensing in cognitive sensor networks," *IEEE Trans. Green Commun. and Netw.*, vol. 1, no. 1, pp. 29–39, March 2017.

[28] E. A. Hodgson, G. Brante, R. D. Souza, J. Garca-Fras, and J. L. Rebelatto, "Compensating spectral efficiency loss of wireless rf energy transfer with analog joint source channel coding compression," *IEEE Sens. J.*, vol. 16, no. 16, pp. 6458–6469, Aug 2016.

[29] E. Hodgson, G. Brante, R. Souza, and J. Garcia-Frias, "Non-parametric analog joint source channel coding for amplify-and-forward two-hop networks," in *2017 IEEE International Conference on Acoustics, Speech and Signal Processing (ICASSP)*, March 2017, pp. 3674–3678.

[30] N. Zhao, F. R. Yu, H. Sun, and M. Li, "Adaptive power allocation schemes for spectrum sharing in interference-alignment-based cognitive radio networks," *IEEE Trans. Veh. Technol.*, vol. 65, no. 5, pp. 3700–3714, May 2016.

[31] X. Li, N. Zhao, Y. Sun, and F. R. Yu, "Interference alignment based on antenna selection with imperfect channel state information in cognitive radio networks," *IEEE Trans. Veh. Technol.*, vol. 65, no. 7, pp. 5497–5511, July 2016.

[32] J. P. B. Nadas, R. D. Souza, M. E. Pellenz, G. Brante, and S. M. Braga, "Energy efficient beacon based synchronization for alarm driven wireless sensor networks," *IEEE Signal Process Lett.*, vol. 23, no. 3, pp. 336–340, March 2016.

[33] B. Nazer and M. Gastpar, "Compute-and-forward: Harnessing interference through structured codes," *IEEE Trans. Inf. Theory*, vol. 57, no. 10, pp. 6463–6486, Oct 2011.

[34] M. Goldenbaum, H. Boche, and S. Staczak, "Harnessing interference for analog function computation in wireless sensor networks," *IEEE Trans. Signal Process.*, vol. 61, no. 20, pp. 4893–4906, Oct 2013.

[35] A. Kortke, M. Goldenbaum, and S. Staczak, "Analog computation over the wireless channel: A proof of concept," in *IEEE SENSORS 2014 Proceedings*, Nov 2014, pp. 1224–1227.

[36] O. Abari, H. Rahul, and D. Katabi, "Over-the-air function computation in sensor networks," *CoRR*, vol. abs/1612.02307, 2016. [Online]. Available: http://arxiv.org/abs/1612.02307

[37] J. G. Proakis and D. K. Manolakis, *Digital Signal Processing (4th Edition)*. Upper Saddle River, NJ, USA: Prentice-Hall, Inc., 2006.

[38] O. Abari, H. Rahul, D. Katabi, and M. Pant, "Airshare: Distributed coherent transmission made seamless," in *2015 IEEE Conference on Computer Communications*, April 2015, pp. 1742–1750.

[39] G. Hattab and M. Ibnkahla, "Multiband spectrum access: Great promises for future cognitive radio networks," *Proc. IEEE*, vol. 102, no. 3, pp. 282–306, March 2014.